Analog Electronic Cochlea Design Using Multiplexing Switched-Capacitor Circuits

Jenn-Chyou Bor and Chung-Yu Wu, *Member, IEEE*

***Abstract*— A new design methodology is proposed to realize a real cochlea using the multiplexing switched-capacitor (SC) circuits. The proposed technique is based upon the transmission-line model proposed by Zwislocki [5]. At the cost of the increase in the number of clock phases, the decay rate in the transition region of the filter section can be increased by adding only a few components. Therefore, the components and chip area of the designed silicon cochlea can be small. An experimental chip containing four filter sections has been designed and fabricated. The measured frequency responses from the 32-section cochlea formed by cascading nine fabricated chips are consistent with both theoretical calculation results and observed behavior of a real cochlea. Moreover, the designed silicon cochlea has the dynamic range of 67 dB in each section and a low sensitivity to process variations. Thus it is suitable for VLSI (very large scale integration) implementation with the associated neural network.**

I. Introduction

ONE approach to develop a speech recognizing system with human-like ability is to design an electronic neural system that mimics the behavior of the human auditory nervous system. To build such a system, the first step is to implement an analog electronic cochlea making use of the current knowledge about the cochlear structure and function. The first electronic cochlea was proposed by Lyon and Mead in 1988 [1]. In their design, variable-Q second-order lowpass filters realized by transconductance amplifiers are cascaded to simulate most of the important qualitative effects of the real cochlea. Since the filter circuits are operated in the subthreshold region, the exponentially varying stiffness along the length of the cochlea can be easily implemented by using a linearly changed bias voltage. Besides, the power consumption is very low. Based upon subthreshold transconductance-C design techniques as in [1], improved versions have been proposed [2]–[4]. Among them [2]–[4], the approach in [3] is to implement the electronic cochlea from the transmission-line model [5] with the impedance of the transmission line directly simulated by the transconductance-C circuits. More recently, the cascaded switched-current biquads are proposed to implement the cochlea [6].

Generally the major cochlear function is equivalent to that of a filter system where many filter sections with very sharp decay in the filter transition region are connected in cascade. In the implementation of the filter section with the required decay of 50–500 dB/octave [4], one approach is to cascade less low-order filter stages. This reduces the number of cascaded stages in the filter system. But the required sharp transition response is sacrificed and thus some characteristics of the human cochlea system may be lost. The other approach is to cascade many low-order filter stages to realize a single section. This could achieve the required sharp transition response, but the inherent nonideal effects such as component mismatches and device finite output resistance in each stage may be more easily accumulated through the cascaded sections to degrade the performance of the filter system. In these two approaches, great design efforts are required to obtain a good compromise between cascaded stage number and filter response.

In this paper, a new design methodology is proposed which can be used to design a single-stage filter section with a sharp transition region. The major design technique is the multiplexing switched-capacitor (SC) circuit technique [7], [8] which efficiently decreases the cascaded stage number of the filter section with the increasing clock phases. Although only the SC circuits are designed in this paper, the proposed design methodology can be applied to the switched-current circuits as well.

In the proposed design methodology, the cochlear model to be implemented is the transmission-line model [5]. But the design technique is different from that in [3]. In the proposed design methodology, the nonlinear two-dimensional (2-D) partial differential equation which is utilized to represent the behavior of the cochlear model, is first changed into several linear one-dimensional (1-D) difference equations by applying the principles of discrete-time signal processing and variable transformation. Based upon the state-variable method, these 1-D difference equations are implemented by the SC circuits to form a filter section. To decrease the components used in these circuits, the multiplexing technique is used. Basically the frequency response of the multiplexing SC circuit as a filter section is a lowpass function with pseudoresonance [9] and sharp decay slope in the transition region. The peak gain of the filter section can be tuned by adjusting the capacitor ratios. The exponentially decreasing cutoff frequencies of the cascaded filter sections can be realized by adjusting the capacitor ratios and downsampling the clock frequency. Cascading many filter sections with suitable peak gains and cutoff frequencies can realize most of the important qualitative effects of real cochleas.

In Section II, the function of the auditory periphery and the cochlear model is described. Model simplifications are

Manuscript received January 6, 1994; revised December 8, 1994 and July 5, 1995. This work was supported by the National Science Council, Taiwan, ROC, under Contract NSC83-0416-E009-006, and Telecommunication Laboratory, Taiwan, ROC, under Contract Y80042.

The authors are with the Department of Electronics Engineering and Institute of Electronics, Integrated Circuit and System Laboratory, National Chiao Tung University, Hsinchu, Taiwan 300, Republic of China.

Publisher Item Identifier S 1045-9227(96)00179-8.

also presented in this section. In Section III, the method to implement the simplified model is presented. First, the simplified model is transformed into the state-variable diagram and its basic functions are realized by the SC circuits. Then the whole circuit of the filter section of the basilar membrane can be formed by using the basic SC circuits. By cascading the filter sections, the electronic cochlea can be realized. The experimental results are shown in Section IV. From the comparisons with the simulation results and the data measured from the real cochlea, it can be shown that the design circuits can satisfy the requirement of the frequency response of the cochlea. Finally, the conclusion is given in Section V.

II. Cochlear Model and Modification

The auditory periphery is composed of the outer ear, the middle ear, and the cochlea. The function of the outer ear is to collect sound signal from the outside world, whereas that of the middle ear is to reduce transfer efficiency when the sound signal is too loud. The function of the cochlea is the most complicated and important one. The simplified schematic illustration of the cochlea is shown in Fig. 1(a) [10]. The building blocks of the cochlea are the basilar membrane, the inner hair cells, and the outer hair cells; their relations with other parts of the auditory nervous system are also shown in Fig. 1(b). In general, the basilar membrane can be treated as the processing unit of the cochlea. The sound signal coupled from the middle ear travels along it and is processed by many lowpass filter sections with the sharp decay slope in the transition region. Since the basilar membrane is a nonuniform medium, the cutoff frequency of the lowpass filter section varies at different positions. Basically, the variation of the cutoff frequency with the location of the basilar membrane can be approximated by an exponential decay function. The inner hair cells distributed along the basilar membrane are the output interface units of the cochlea. They detect the basilar membrane displacement and transfer it into the neural signal. On the other hand, the outer hair cells act as the control units of the cochlea, which adjust the damping of the basilar membrane according to the signal level. If the sound signal which travels along the basilar membrane is too weak to hear, the control signal from the nervous system will inform the outer hair cells to provide positive feedback for the membrane to amplify this signal.

In the past years, there have been many models proposed to characterize the behavior of the cochlea. The cochlear model investigated in this paper is the transmission-line model first proposed by Zwislocki [5]. This model uses simple differential equations to represent the function of the cochlea. It can characterize the essential feature of the traveling wave on the basilar membrane.

Under some assumptions, the cochlea can be represented by a transmission line with distributed parallel and series impedances which vary continuously with distance x along the basilar membrane. A section of the transmission line of length Δx is shown in Fig. 2 [10]. The series impedance $Z(x)\Delta x$ is associated with the fluid moving in the longitudinal (or x) direction while the parallel admittance $Y(x)\Delta x$ is associated

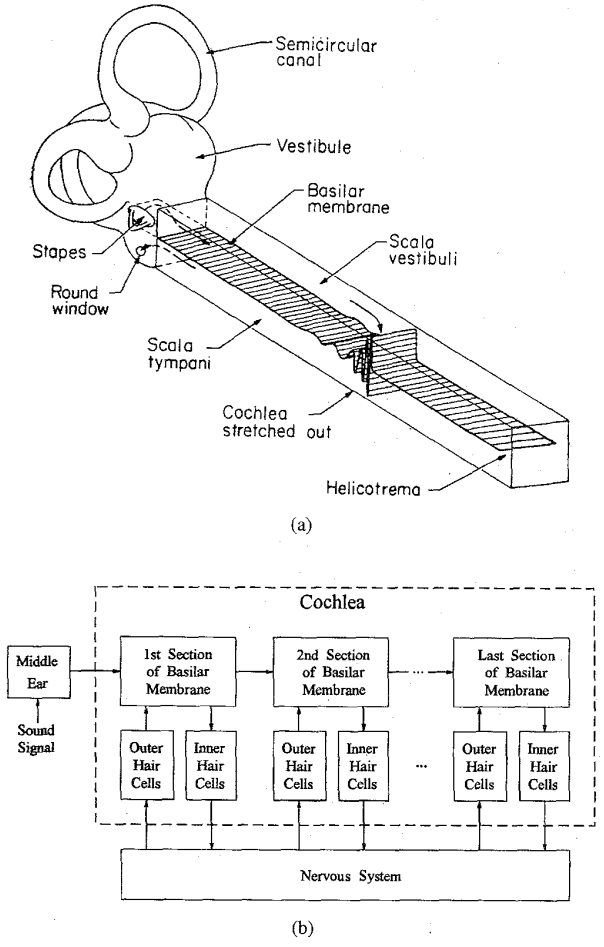

Fig. 1. (a) The simplified schematic illustration of the cochlea [10]. (b) The building blocks of the cochlea and their relations with other parts of the auditory nervous system.

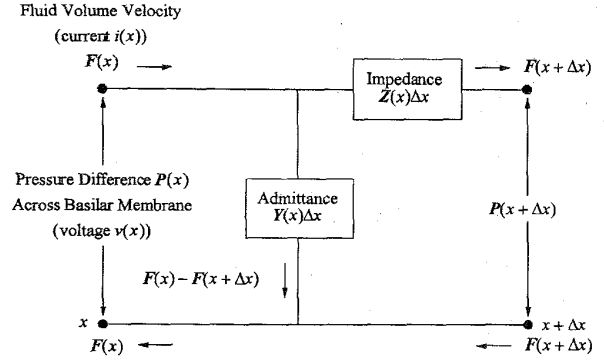

Fig. 2. A section of the basilar membrane of length Δx [10].

with the transverse motion of the basilar membrane and the fluid as its load. The pressure difference across the basilar membrane and the fluid volume velocity are denoted by $\boldsymbol{P}(x)$ and $\boldsymbol{F}(x)$, respectively. Although not explicitly indicated, $\boldsymbol{Z}$, $\boldsymbol{Y}$, $\boldsymbol{P}$, and $\boldsymbol{F}$ also depend on the angular frequency ω. Since the pressure difference $\boldsymbol{P}$ is corresponding to the voltage in an electrical transmission line, whereas the fluid volume velocity

$\boldsymbol{F}$ is corresponding to the current, the behavior of the cochlea can be described by the following [10]:

$$\boldsymbol{F}(x)-\boldsymbol{F}(x+\Delta x)\approx \boldsymbol{P}(x)\boldsymbol{Y}(x)\Delta x, \tag{1a}$$

$$\boldsymbol{P}(x)-\boldsymbol{P}(x+\Delta x)\approx \boldsymbol{F}(x+\Delta x)\boldsymbol{Z}(x)\Delta x. \tag{1b}$$

Decoupling the above equations, we have [10]

$$\frac{d^2\boldsymbol{P}}{dx^2}-\frac{d\ln \boldsymbol{Z}}{dx}\frac{d\boldsymbol{P}}{dx}-\boldsymbol{YZP}=0, \tag{2a}$$

$$\frac{d^2\boldsymbol{F}}{dx^2}-\frac{d\ln \boldsymbol{Y}}{dx}\frac{d\boldsymbol{F}}{dx}-\boldsymbol{YZF}=0. \tag{2b}$$

Also, the basilar membrane displacement Δ can be represented as [10]

$$\Delta=\frac{\boldsymbol{YP}}{i\omega} \tag{3}$$

where ω is the angular frequency and $i=\sqrt{-1}$. Using the approximation method proposed by Zweig [10] and assuming [10]

$$\boldsymbol{Z}=i\omega L_1$$

and

$$\boldsymbol{Y}=(i\omega L+R+1/i\omega C)^{-1}$$

where L_1, L, R, and C which only depend on distance x are the equivalent inductive, resistive, and capacitive components in the transmission-line model, (2a) can be solved and the basilar membrane displacement can be obtained. The comparison of the basilar membrane displacement predicted by this solution with the experimental measurement [11] is described in [10]. The result of this model agrees with the measured behavior of the real cochlea.

Using the above expressions of $\boldsymbol{Y}$ and $\boldsymbol{Z}$ and the inverse Fourier transformation to transform (2a) from the frequency domain to the time domain, it can be rewritten as

$$\left(\frac{d^2P}{dx^2}+RC\frac{d^3P}{dt\,dx^2}+LC\frac{d^4P}{dt^2\,dx^2}\right)-\frac{d\ln L_1}{dx}\left(\frac{dP}{dx}+RC\frac{d^2P}{dt\,dx}+LC\frac{d^3P}{dt^2\,dx}\right)-L_1C\frac{d^2P}{dt^2}=0 \tag{4}$$

where $P=P(t,x)$ is the pressure difference in the time domain. Since the coefficients of the above equation depends on distance x, it is a nonlinear 2-D partial differential equation. It is impossible to implement such an equation directly. Therefore, some modification should be applied to (4) to simplify it.

To modify (4), the first step is to change it into a set of linear equations. If the basilar membrane is divided into N cascading sections and the range of variable x is limited to a small value x_u in each section, (4) can be simplified and reexpressed by many linear partial differential equations with suitable constant coefficients to represent the functions of these cascaded sections. The difference between the response of (4) and the cascaded responses of these linear equations can be neglected as x_u is small enough. The simplified equation in the kth section is given by

$$\frac{d^2P}{dx^2}+\alpha 1_k\frac{d^3P}{dt\,dx^2}+\alpha 2_k\frac{d^4P}{dt^2\,dx^2}+\alpha 3_k\frac{dP}{dx}+\alpha 4_k\frac{d^2P}{dt\,dx}+\alpha 5_k\frac{d^3P}{dt^2\,dx}+\alpha 6_k\frac{d^2P}{dt^2}=0 \tag{5}$$

where $\alpha 1_k$, $\alpha 2_k$, $\alpha 3_k$, $\alpha 4_k$, $\alpha 5_k$, and $\alpha 6_k$ are constant coefficients, $1\le k\le N$, and $(k-1)x_u<x\le kx_u$.

Based on the observation that the properties of the basilar membrane change slowly with x, its frequency response is scale-invariant [1], and there is essentially no phase delay in the pressure along the basilar membrane [12], it can be realized that the frequency responses of two adjacent points along the x dimension are almost the same except that the cutoff frequencies are slightly different. Thus the x derivatives of P is nearly zero in the passband and stopband regions and small in the transition region. This leads to very small second-order x derivatives and they can be neglected. With the neglect of second-order x derivatives, the complexity of (5) is reduced significantly. To simulate the function of the outer hair cells, the dP/dt term is added to (5). By adjusting the coefficient of this term, the pressure difference in some frequency ranges can be amplified to the required level. The resulting new equation in the kth section is given by

$$\frac{dP}{dx}+a_k\frac{d^2P}{dt\,dx}+b_k\frac{d^3P}{dt^2\,dx}+c_k\frac{dP}{dt}+d_k\frac{d^2P}{dt^2}=0 \tag{6}$$

where a_k, b_k, c_k, and d_k are constant coefficients. Transforming (6) into the frequency domain by using the Fourier transformation, a linear differential equation which only contains the first x derivative can be obtained and its solution can be easily solved as

$$\boldsymbol{P}(i\omega,x)=\boldsymbol{P}[i\omega,(k-1)x_u]\cdot\exp\left[\frac{-c_ki\omega-d_k(i\omega)^2}{1+a_ki\omega+b_k(i\omega)^2}(x-kx_u+x_u)\right] \tag{7}$$

where $(k-1)x_u<x\le kx_u$ and $P[i\omega,(k-1)x_u])$ is the input signal of the kth section. Choosing the adequate coefficients and simply setting the basilar displacement as $\Delta=\boldsymbol{P}\cdot i\omega\cdot\sqrt{b_k}$, the frequency response of the displacement can be obtained from (7) as shown in Fig. 3. As compared with the data in [10] and [11], this result has the same qualitative properties of the shallow low-frequency slope, the sharp high-frequency slope, and the pseudoresonance. Moreover, the gain near the cutoff frequency can be tuned by changing the coefficient c_k. This is the function of the outer hair cells. Although the decay slope in the high-frequency range will become flat, the gain is very small and will not affect the cascaded response. From the above comparison, it can be seen that the approximation error of (6) is tolerable and it can characterize the essential feature of a real cochlea.

III. Realization of the Cochlear Model

A. Sampling and Mapping

To implement (6) using SC circuits, the state-variable diagram [13]–[14] needs to be constructed first. Since (6) is a 2-D partial differential equation, there are four basic

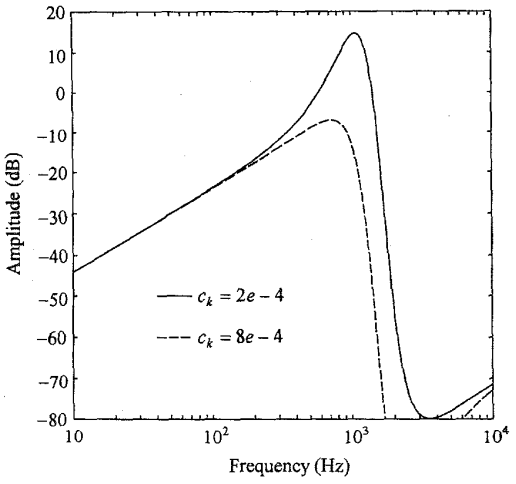

Fig. 3. The simplified basilar membrane displacement predicted by (6) where $a_k = 1e-4$, $b_k = 1e-8$, and $d_k = 1e-7$.

functions required to form the state-variable diagram. These functions are the time differentiation $dP(t, x)/dt$, time integration $\int P(t, x)\,dt$, distance differentiation $dP(t, x)/dx$, and distance integration $\int P(t, x)\,dx$. By using the clock with period T_t to sample the data in the time domain, the clock with period T_x to sample the data in the distance domain, and the backward Euler formula to approximate both differentiation and integration, the basic functions can be expressed as

$$D_t[P(mT_t, nT_x)] = \frac{1}{T_t}[P(mT_t, nT_x) - P(mT_t - T_t, nT_x)] \quad (8a)$$

$$I_t[P(mT_t, nT_x)] = T_t \sum_{i=0}^{m} P(iT_t, nT_x) \quad (8b)$$

$$D_x[P(mT_t, nT_x)] = \frac{1}{T_x}[P(mT_t, nT_x) - P(mT_t, nT_x - T_x)] \quad (8c)$$

$$I_x[P(mT_t, nT_x)] = T_x \sum_{j=0}^{n} P(mT_t, jT_x) \quad (8d)$$

where $D_t[\cdot]$ represents time differentiation operator, $I_t[\cdot]$ represents time integration operator, $D_x[\cdot]$ represents distance differentiation operator, and $I_x[\cdot]$ represents distance integration operator.

Although the discrete-signal equations of these basic functions have been derived, they are all 2-D difference equations and very difficult to implement without complex circuits. Therefore, it is necessary to transfer $P(mT_t, nT_x)$ into 1-D sequences so that the conventional SC design method can be applied to the realization of (8a)–(8d). Assume the range of variable x in each section of the basilar membrane is sampled into N_x points, i.e., $x_u = N_x T_x$. In each section, there are only limited points of data when the variable t is fixed. The discrete signals in the kth section can be expressed as

$$P(mT_t, nT_x), \quad (k-1)N_x + 1 \le n \le kN_x.$$

If the $N_x - 1$ points, $P(mT_t, nT_x)$, $(k-1)N_x + 2 \le n \le kN_x$ are mapped into the time domain and inserted between $P(mT_t, (k-1)N_x T_x + T_x)$ and $P(mT_t + T_t, (k-1)N_x T_x + T_x)$, the 2-D data sequence $P(mT_t, nT_x)$ in the kth section can be transformed into the 1-D data sequence. The relationship of the new data sequence and the original signal is defined as

$$Q_k[(m-k+1)N_x + n] \equiv P(mT_t, nT_x), \quad (k-1)N_x + 1 \le n \le kN_x \quad (9)$$

where the 1-D data sequence Q_k is used to represent the mapping signal from the kth section and the sampling period of Q_k is T_t/N_x.

B. Realization of the Basic Functions

By using the new data sequence Q_k, (8a)–(8d) can be transformed into 1-D equations and implemented by SC circuits easily. Since the combination with differentiators and integrators usually makes the capacitor ratios of SC circuit smaller and the implementation of time differentiation is simpler than that of time integration, the function of D_t and I_x are used to construct the state-variable diagram. The implementation of these two functions by SC circuits is described in the following.

1) Time Differentiation: Substituting the new data sequence Q_k for $P(mT_t, nT_x)$ in (8a), it can be transformed into 1-D equation as

$$D_t[P(mT_t, nT_x)] = \frac{1}{T_t}Q_k[(m-k+1)N_x + n] - Q_k[(m-k)N_x + n)]. \quad (10)$$

Applying the z-transformation to the above equation, the transfer function of time differentiation can be obtained as

$$H_{TD}(z) = \frac{1}{T_t}(1 - z^{-N_x}). \quad (11)$$

This transfer function can be designed as a FIR (finite impulse response) filter, but this would result in the increase of components in the circuit. Here, the multiplexing technique is introduced to implement the time differentiation. The resulting SC circuit and the clock waveforms are shown in Fig. 4 where the core structure of the SC differentiator proposed in [15] and [16] has been used. In this circuit, the capacitor array is controlled by N_x clocks and every capacitor is recharged in turn. Therefore, N_x points of the past data can be held in this array and the function of time differentiation can be realized.

2) Distance Integration: By using the new data sequence Q_k instead of $P(mT_t, nT_x)$, (8d) can be changed into

$$I_x[P(mT_t, nT_x)] = T_x \sum_{j=1}^{n-(k-1)N_x} Q_k(mN_x + j) + I_x[P_{k0}] \quad (12)$$

where $(k-1)N_x + 1 \le n \le kN_x$ and $I_x[P_{k0}] = I_x[P(mT_t, (k-1)N_x T_x)]$ is the initial condition of I_x which is determined by the previous section. Applying the

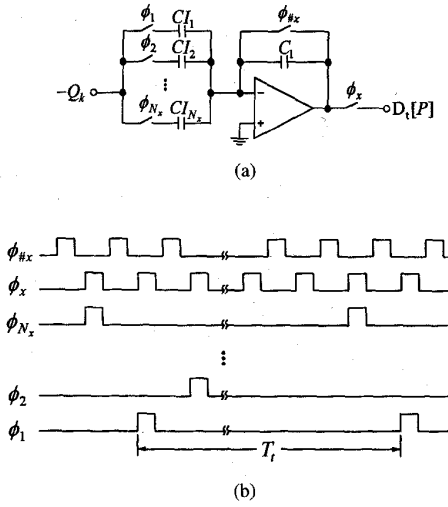

Fig. 4. (a) The time differentiation circuit and (b) the associated clock waveforms where $T_x = x_u/N_x$.

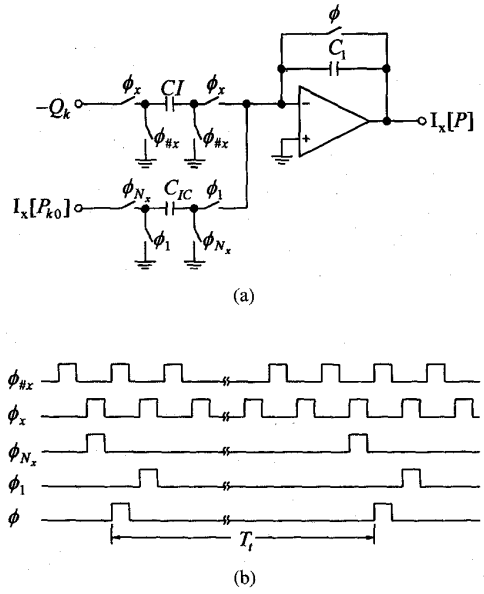

Fig. 5. (a) The distance integration circuit and (b) the associated clock waveforms where $T_x = x_u/N_x$.

z-transformation, the transfer function of distance integration is given by

$$H_{DI} = \frac{T_x}{1 - z^{-1}}. \tag{13}$$

This is the same as the ordinary form of integration. The distance integration, however, must restart with the new initial condition after N_x points. Thus a clock is used to reset the stored charge on capacitors. The modified circuit and the associated clock waveforms are shown in Fig. 5 where the backward-Euler SC integrator [17] is adopted as the core structure and the initial condition is input from the branch of the capacitor C_{IC}.

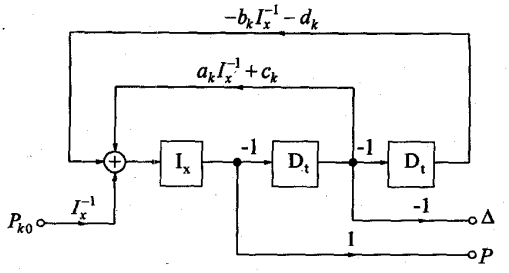

Fig. 6. The state-variable diagram of (6).

C. Entire Circuit of One Section

By using the time differentiation D_t and the distance integration I_x, the state-variable diagram of (6) is constructed as shown in Fig. 6. Applying the above SC circuits to this state-variable diagram, the whole circuit can be developed and shown in Fig. 7 where the pressure difference P and the basilar membrane displacement Δ are taken from the output of the op-amps $E1$ and $E3$, respectively. The value of N_x is chosen as four, which is adequate to make the approximation valid and obtain the required sharp decay slope in the filter transition region. In this case, the design equation of the capacitor ratios as functions of the coefficients of (6) are shown below

$$\begin{aligned}
\frac{CD_{2i}}{C_2}\frac{CA_3}{C_3}\frac{CA_{31}}{C_1} &= \frac{a_k}{T_t}, \\
\frac{CD_{2i}}{C_2}\frac{CA_3}{C_3}\frac{CI_{31}}{C_1} &= \frac{T_x c_k}{T_t}, \\
\frac{CD_{2i}}{C_2}\frac{CD_{4i}}{C_4}\frac{CA_{41}}{C_1} &= \frac{b_k}{T_t^2}, \\
\frac{CD_{2i}}{C_2}\frac{CD_{4i}}{C_4}\frac{CI_{41}}{C_1} &= \frac{T_x d_k}{T_t^2}, \\
\frac{C_{IN}}{C_1} &= 1
\end{aligned}$$

where $1 \le i \le 4$.

In the SC circuit, the aliasing error is a major concern and must be decreased as much as possible by choosing the suitable clock period. Since this circuit is derived from the 2-D partial differential equation, there are two clock periods T_t and T_x which must be chosen very carefully to avoid the aliasing error. The clock period T_t can be determined from the frequency bandwidth of input signal. As to the clock period T_x, the aliasing error from the x domain can be reduced as T_x decreases. This will, however, increase the data points N_x and the required clocks and components used in a single section. The choice of T_x is a trade-off between the aliasing error from the x domain and the circuit complexity. The comparison between discrete-time frequency responses with different T_x and ideal one is shown in Fig. 8. This figure indicates that the aliasing error from the x domain mainly affects the decay speed in the transition region. Therefore, T_x can be determined by the required decay speed.

Ideally, since the feedback to the op-amp $E1$ are all negative, it should have no stability problem. Due to the time delay of the global negative feedback path through the

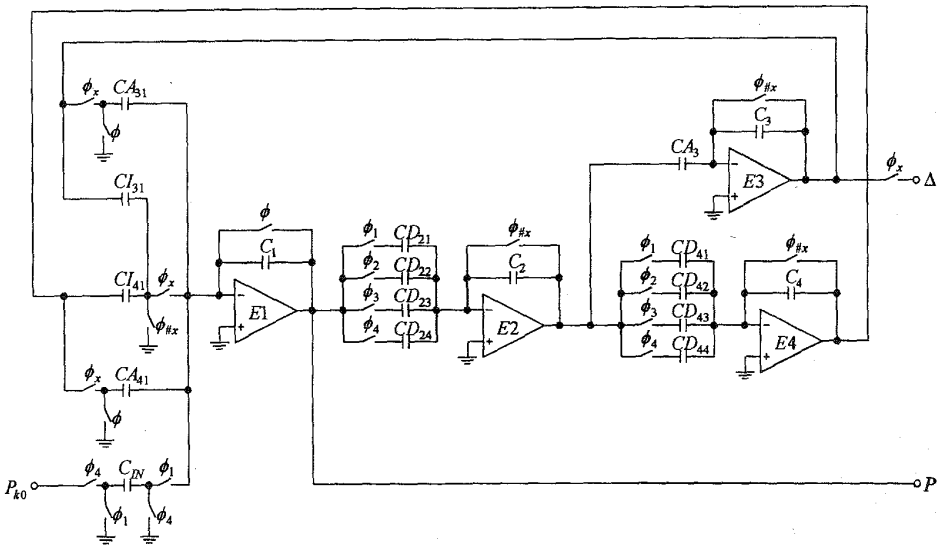

Fig. 7. The SC circuit to represent one section of the basilar membrane where $N_x = 4$.

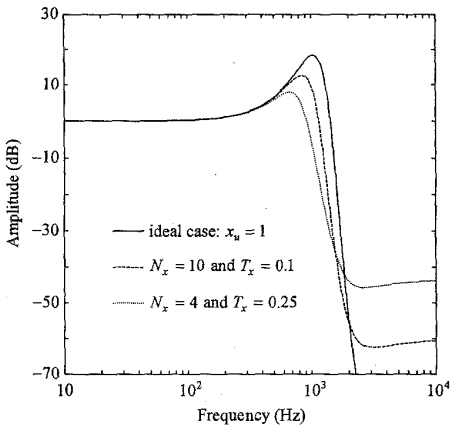

Fig. 8. The comparison between the discrete-time frequency responses of (6) with two different T_x and the ideal case where $a_k = 1e-4, b_k = 1e-8, c_k = 2e-4$, and $d_k = 1e-7$.

op-amps $E2$, $E3$, and $E4$, however, the circuit still has the probability to oscillate if the global negative feedback is large enough. To solve this problem, some redundant capacitors are added to the circuit to increase the local negative feedback. The resultant circuit is shown in Fig. 9. In this modified circuit, the capacitors CA_{11} and CI_{11} are used to increase the local negative feedback of the op-amp $E1$, whereas the capacitor CA_{14} is used to offset the charges provided by CA_{11} and CI_{11} and make the overall transfer function unchanged. Although the feedback provided by CA_{14} is positive, the modified circuit does not have the stability problem since the negative feedback is large enough to cancel out the effect of the positive feedback. The HSPICE (a circuit simulator of Meta Software, Inc.) simulation result is shown in Fig. 10. It can be seen that the overshooting of the modified circuit is lower than that of the original circuit. Therefore, the modified circuit is more stable than the original one.

Note that ideally CA_{14} can entirely cancel out the charges provided by CA_{11} and CI_{11}. Since the charges of CA_{14} propagate through the op-amp $E4$, the amount will be reduced slightly due to the finite gain of $E4$. This will result in the gain degradation in the passband region. As shown in Fig. 11, the gain deviation from unity in the passband region is more serious than that of the original circuit. Although this error can be reduced by raising the op-amp gain, the required gain to obtain the ideal response is very high. Therefore, it is more efficient to increase the capacitor ratio C_{IN}/C_1 for gain compensation. The gain of the transfer function can be increased as C_{IN}/C_1 increases. Thus the passband gain deviation can be compensated. The resulting frequency response is also shown in Fig. 11 for comparisons.

To implement the basilar membrane, one important thing is to realize the sharp high-frequency cutoff. Besides increasing N_x, this can be accomplished by adjusting the value of the capacitor CA_{31}. The frequency response with different values of CA_{31} is shown in Fig. 12. This figure indicates that the decay curve in the transition region becomes sharper when the value of CA_{31} decreases. Since the required decay slope beyond the cutoff frequency to obtain the desired response is 50–500 dB/octave [4], this requirement can be satisfied by choosing a small value of CA_{31}.

The function of the outer hair cells can be implemented by tuning the value of the capacitor CI_{31}. The frequency response with different values of CI_{31} is shown in Fig. 13. The gain near the cutoff frequency is controlled by the value of CI_{31}. As the value of CI_{31} decreases, the gain is increased while the decay slope in the transition region is kept almost unchanged. This result is similar to the change of the Q-parameter in the second-order filter of the previous design [1]–[4], [6], but the tunable range of the proposed circuit is larger. An effective tunable capacitor can be implemented by the SC circuit shown in Fig. 14. Using the signals A1–A3 to control the switches, the capacitor value can be adjusted from C_0 to $C_0 + 7C_u$. The

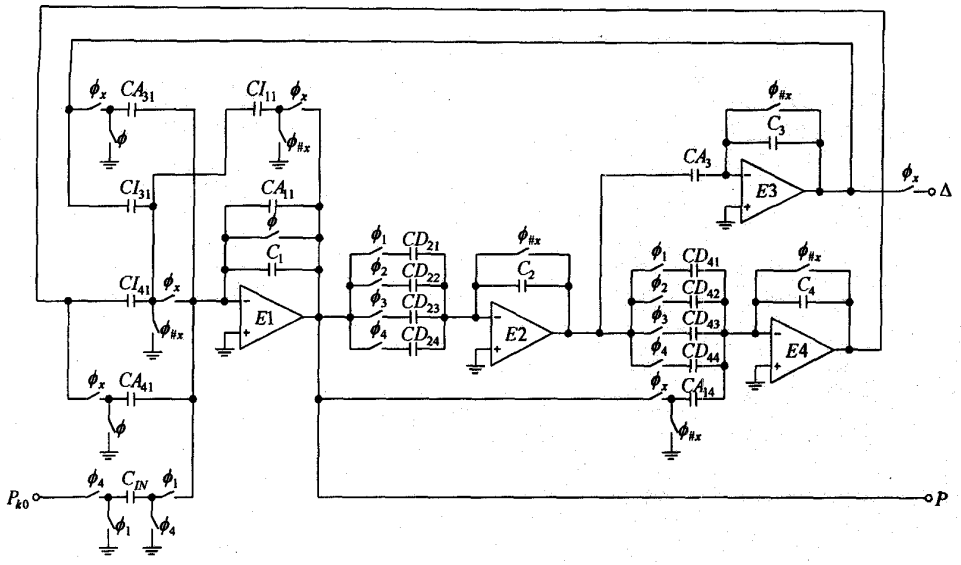

Fig. 9. The modified version of the circuit in Fig. 7. This circuit is more stable.

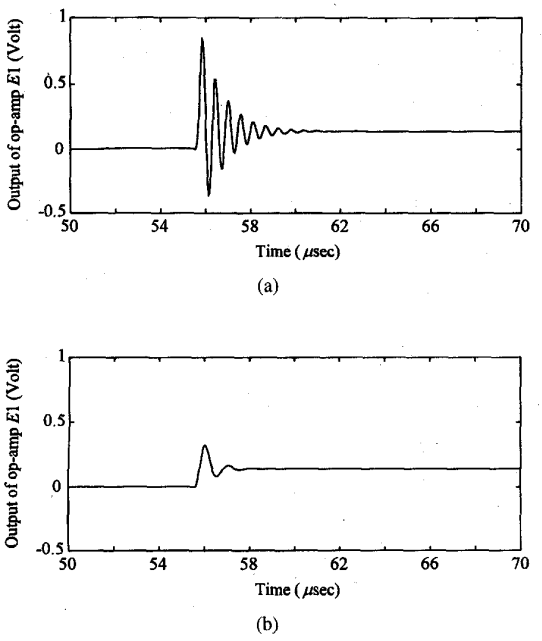

Fig. 10. The transient response from the output of the op-amp $E1$ when ϕ_1 becomes active: (a) the case of the original circuit and (b) the case of the modified circuit where $T_x = T_t = 2e-4$ s, $CA_{11} = 4$ pF, $CI_{11} = 8$ pF, $CA_{31} = 0$ pF, $CI_{31} = 1$ pF, $CA_{41} = 4$ pF, $CI_{41} = 8$ pF, and other capacitors are 1 pF.

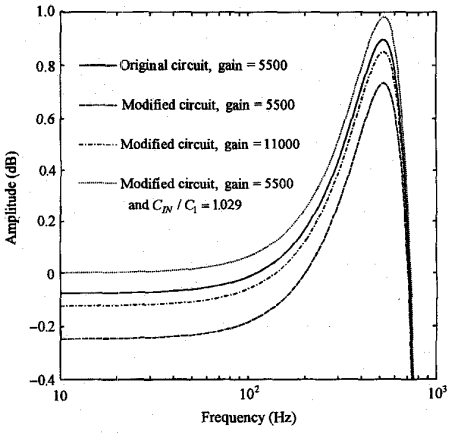

Fig. 11. The comparison between the frequency responses in the passband region of the original circuit and the modified circuit under some conditions. In this figure, $T_t = 4e-4$, $CI_{31} = 3$ pF, and the values of other unspecified capacitors are the same as those in Fig. 10.

signals to control the outer hair cells are generated from the nervous system as shown in Fig. 1. Therefore, the circuit to generate these control signals is not included in the designed circuit.

The basilar membrane displacement is produced from the output of the op-amp $E3$. It uses the time differentiation to produce the shallow low-frequency slope. The simulation result is shown in Fig. 15. It can be seen that the slope in the cutoff frequency range is 6–12 dB/octave, which satisfies the requirement of the basilar membrane [4].

D. Cochlea Realization

To implement an electronic cochlea, the section circuit in Fig. 9 can be cascaded to achieve the required frequency response and the number of the required sections is equal to the required outputs along the basilar membrane. Since the basilar membrane is modeled as a transmission line with exponentially varying propagation velocity and cutoff frequency, the cutoff frequency scaling factors between two adjacent sections are set to the same value, which is determined by the total amount of the sections and the bandwidth of sound signal. There are two methods to tune the cutoff frequency of the section circuit. In the first method, the capacitor ratios are adjusted to

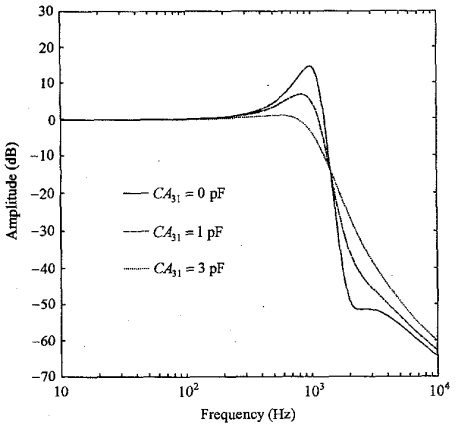

Fig. 12. The simulated frequency response of pressure difference with different values of CA_{31}. The sampling periods and the capacitor values are the same as those in Fig. 11.

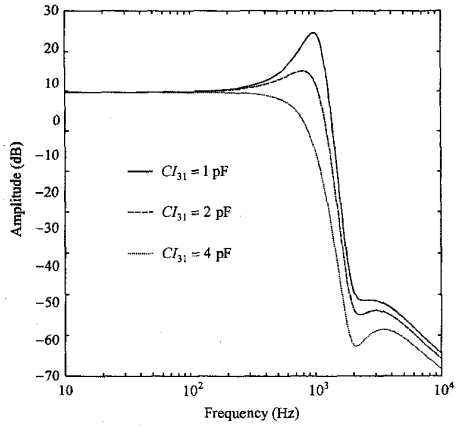

Fig. 13. The simulated frequency response of pressure difference with different values of CI_{31}.

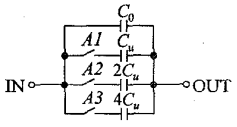

Fig. 14. An effective tunable capacitor.

obtain the required cutoff frequency according to the derived transfer function. This can be done by tuning the capacitor ratios of CD_{2i}/C_2 and CD_{4i}/C_4. The increasing amount of these capacitor ratios is equal to the decreasing amount of the cutoff frequency. When the capacitor ratios becomes too large, the second method is suggested where the sampling period instead of the capacitor ratio is increased to obtain the required cutoff frequency. To simplify the clock generation circuit, the sampling period is increased by integral number only.

For simplicity, we assume that the outer hair cells feed the same amount of positive feedback into all sections of the basilar membrane. Thus the value of the capacitor CI_{31} in each section is controlled by the same signals except that in the front sections. Due to the cascaded structure, the gain near

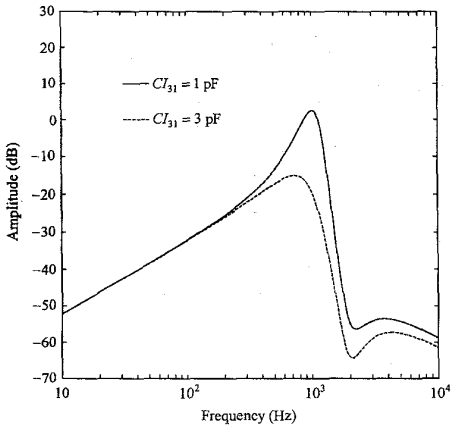

Fig. 15. The simulated frequency response from the output of the op-amp $E3$.

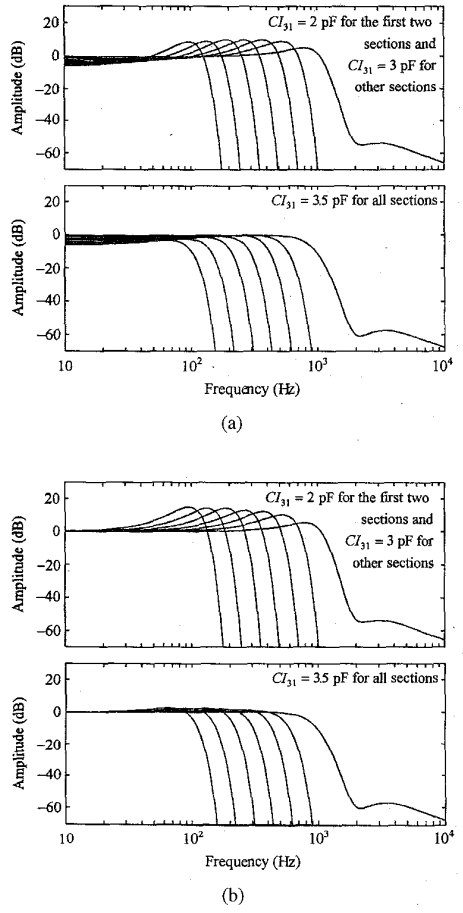

Fig. 16. The simulated pressure differences of seven outputs [the $(1+4n)$th sections, n = 0–6] from the cascaded 28 sections under two CI_{31} tuning conditions: (a) C_{IN} = 1 pF; (b) C_{IN} = 1.029 pF.

the cutoff frequency in the back sections is also determined by that in the previous sections. If the gain of each section is slightly greater than one, the gain peak becomes much higher in the back sections than that in the front sections. To make the frequency response of all sections similar, the value of

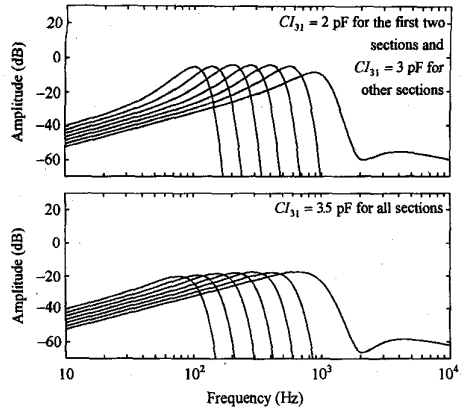

(a)

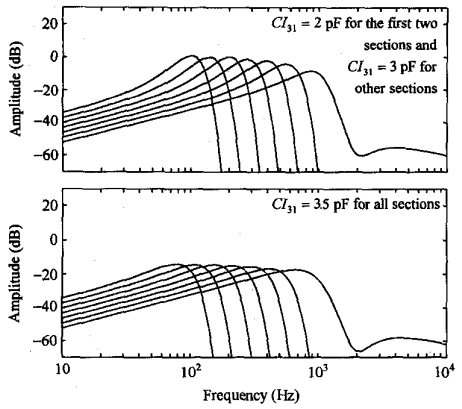

(b)

Fig. 17. The simulated basilar membrane displacements of seven outputs [the $(1 + 4n)$th sections, n = 0–6] from the cascaded 28 sections under two CI_{31} tuning conditions: (a) $C_{IN} = 1$ pF; (b) $C_{IN} = 1.029$ pF.

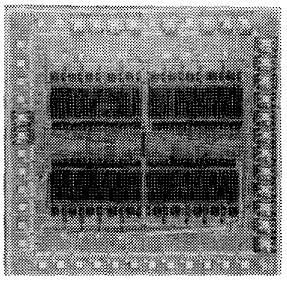

Fig. 18. The chip photomicrograph.

CI_{31} in the front sections should be slightly smaller than that in other sections.

The SWITCAP (a switched-capacitator network analysis program of Columbia University) simulation results of the pressure differences in the cascaded 28 sections under two tuning conditions of CI_{31} are shown in Fig. 16. The outputs are taken from the $(1 + 4n)$th sections, n = 0–6. The scaling factor between two adjacent sections is 1.0905. This figure indicates that the simulated frequency responses have a sharp high-frequency cutoff and exhibit significantly different tuning characteristics under the two tuning conditions. Since the gain

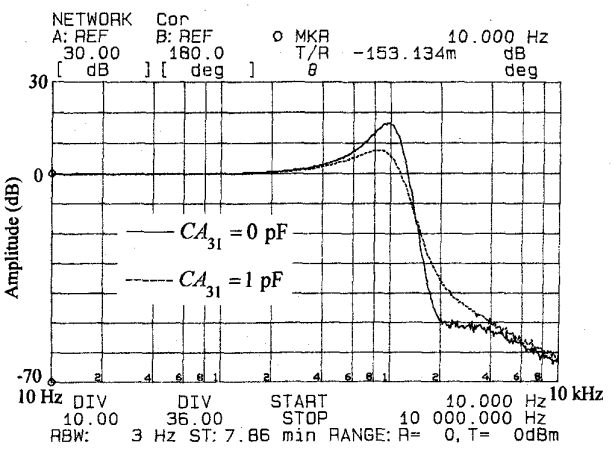

(a)

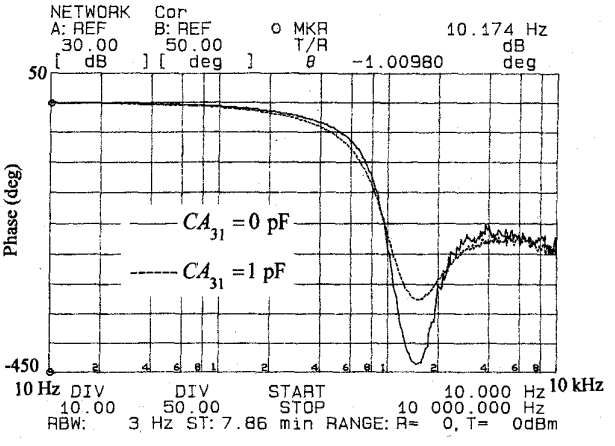

(b)

Fig. 19. The measured (a) amplitude response; (b) phase response of the pressure difference with $CI_{31} = 1$ pF and different values of CA_{31}.

in the passband of each section is slightly less than one due to finite op-amp gain error, the frequency response of the cascaded structure accumulates this error and the gain in the back sections becomes smaller as shown in Fig. 16(a). By slightly increasing the value of the capacitor C_{IN}, this error can be eliminated. The resulting frequency response is shown in Fig. 16(b). The frequency response of the basilar membrane displacement is shown in Fig. 17. As compared to the theoretical results, the consistence is acceptable.

IV. Experimental Results

To verify the designed circuits, an experimental chip is fabricated. The chip photomicrograph is shown in Fig. 18 and its size is 3.5 mm × 3.5 mm. It contains four sections of the circuit shown in Fig. 9 and four unit-gain followers between the outputs of these sections and pads. The op-amps used in the SC circuit are of the simple two-stage type [14]. The capacitors except C_2 and C_4 are implemented by the unit capacitor array with 1 pF unit capacitors. The values of the capacitors CA_{31} and CI_{31} can be tuned from 0–7 pF by three control signals. Both capacitor ratios CD_{2i}/C_2 and CD_{4i}/C_4

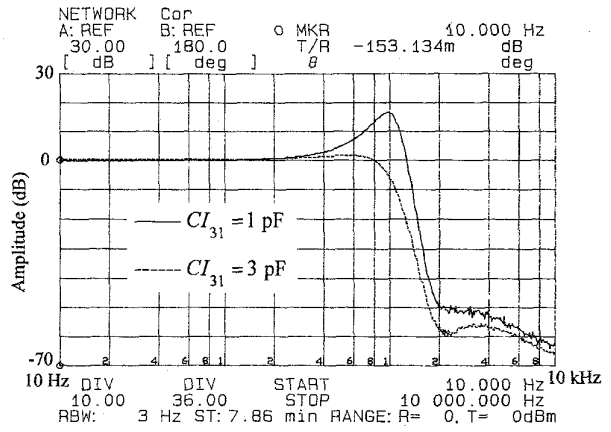

(a)

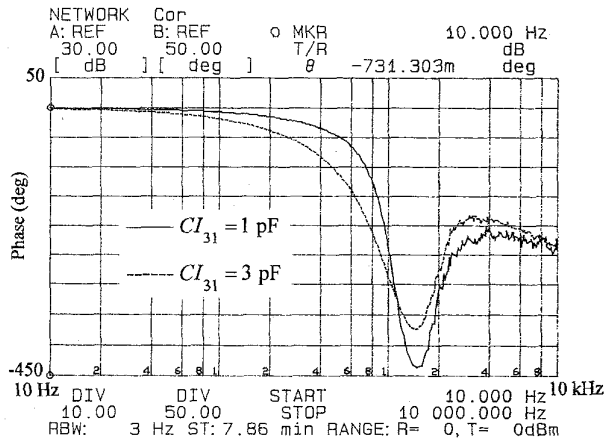

(b)

Fig. 20. The measured (a) amplitude response; (b) phase response of the pressure difference with $CA_{31} = 0$ pF and different values of CI_{31}.

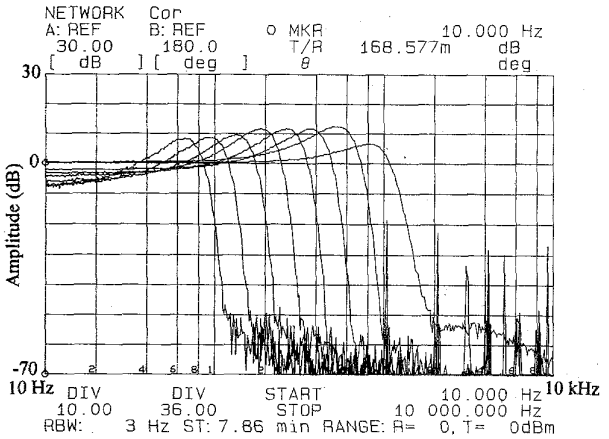

(a)

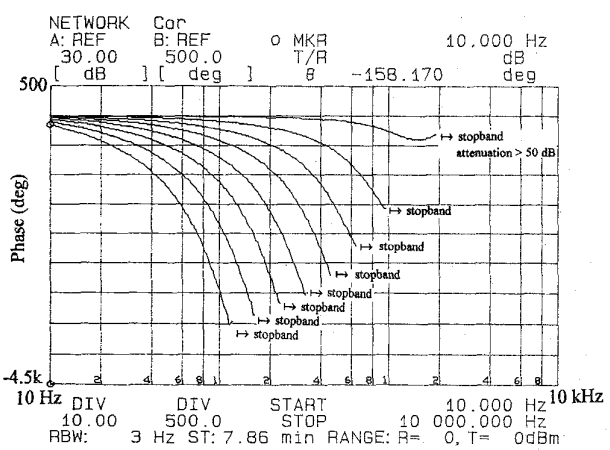

(b)

Fig. 21. The measured (a) amplitude response; (b) phase response of the pressure difference of eight outputs [the $(1 + 4n)$th sections, $n = 0$–7] from 32 sections where $CA_{31} = 0$ pF, $CI_{31} = 2$ pF for the first and second sections and $CI_{31} = 3$ pF for other sections.

in the first section are equal to one and the scaling factor between two adjacent sections is 1.0905 which is realized by reducing the layout sizes of C_2 and C_4 directly. The capacitor ratio C_{IN}/C_1 is equal to one and the number of the total clock phases is seven.

The measured frequency response of the first section under two tuning conditions $CA_{31} = 0$ pF and $CA_{31} = 1$ pF is shown in Fig. 19. It can be seen that the decay slope in the transition region is increased as CA_{31} decreases. This is consistent with the simulation results. Fig. 20 shows the measured frequency response of the first section for CI_{31} equal to 1 pF and 3 pF. As the value of CI_{31} decreases, the gain near the cutoff frequency is increased, but the decay slope in the transition region remains nearly unchanged. This is consistent with the SWITCAP simulation results. Thus the proposed circuit can be used to mimic the function of the outer hair cells.

Under the conditions that the total harmonic distortion is below 1%, $CA_{31} = 0$ pF, $CI_{31} = 3$ pF, the bandwidth is 1 kHz, and the power supply is ± 3 V, the maximum output of a single section circuit is 4 V_{pp}. The measured output noise level is 1.64 mV_{pp}. Therefore, the dynamic range of a single section circuit is 67 dB. Since the dynamic range of the wide-range-input transconductance amplifier in [2] is about 62.6 dB and significantly less when cascading several amplifier stages to form a single section, the proposed circuit has a larger dynamic range.

An experimental basilar membrane with 32 sections is realized by cascading nine fabricated chips where only two sections out of four are used in the first and second chips. Thus the values of CI_{31} in the first two chips can be independently tuned. The sampling periods T_t of the first–fourth sections and the fifth–eighth sections are 40 and 60 μs, respectively, and doubled after every eight sections. The value of CA_{31} is set to 0 pF and the value of CI_{31} is set to 3 pF in all sections except the first and second sections where the value is 2 pF. Fig. 21(a) and (b) shows the frequency responses of the pressure difference which are measured from the first section of the first and third–ninth chips. In Fig. 21(a), the peaks in the high frequency stopband are due to the coupling from the sampling clocks. They do not influence the correctness of the overall function. In Fig. 21(b), only the phase response in the

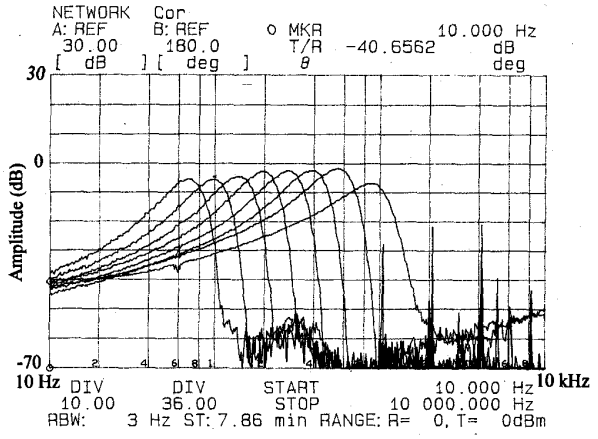

(a)

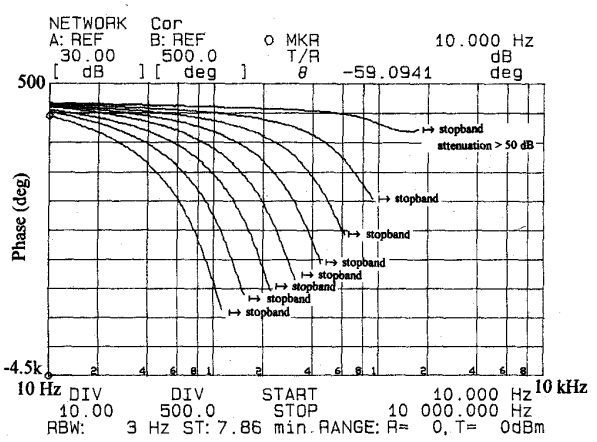

(b)

Fig. 22. The measured (a) amplitude response; (b) phase response of the basilar membrane displacement of eight outputs (the $(1+4n)$th sections, n = 0–7) from 32 sections where $CA_{31} = 0$ pF and $CI_{31} = 2$ pF for the first and second sections and $CI_{31} = 3$ pF for other sections.

passband and transition regions are presented. It can be seen from these figures that the measured responses are consistent with the simulation results. The corresponding basilar membrane displacement is shown in Fig. 22. It has the shallow low-frequency slope and sharp high-frequency slope which are consistent with the data measured from a real cochlea [11].

The errors between measured values and theoretical values of peak gains and peak frequencies of the basilar membrane displacement are listed in Table I(a). The theoretical values are obtained from the ideal discrete-time transfer functions. Since the finite op-amp gain mentioned in Section III-D affects the overall filter gains, the peak gain values in the error calculation are the relative peak gains with respect to the passband gains of the pressure difference, so that the error due to finite op-amp gain are eliminated. It can be seen the peak gain errors are large in the back sections. This is mainly due to the finite bandwidth of the op-amps [13]. In the transient operation, the finite bandwidth of the op-amps affects the final settled results and leads to peak gain degradation. Thus the resultant peak gain errors are rather larger than that of the cutoff frequencies.

TABLE I

(a) THE ERRORS OF THE MEASURED PEAK GAINS AND PEAK FREQUENCIES OF THE BASILAR MEMBRANE DISPLACEMENT FROM THE THEORETICAL VALUES. (b) THE ERRORS OF THE PEAK GAINS AND PEAK FREQUENCIES OF THE BASILAR MEMBRANE DISPLACEMENT FROM THE THEORETICAL VALUES WHERE THE COEFFICIENTS c_k FOR ALL SECTIONS ARE SCALED BY A FACTOR OF 0.96

	1st section	5th section	9th section	13th section	17th section	21th section	25th section	29th section
peak gain error	19.0%	57.6%	65.6%	62.9%	69.3%	57.1%	69.2%	65.9%
peak frequency error	0.00%	1.74%	7.15%	3.51%	5.32%	3.06%	7.15%	9.02%

(a)

	1st section	5th section	9th section	13th section	17th section	21th section	25th section	29th section
peak gain error	10.0%	7.93%	9.15%	4.10%	5.54%	-3.03%	3.44%	1.37%
peak frequency error	0%	-3.39%	1.74%	-1.71%	0.00%	-2.15%	1.74%	3.51%

(b)

Due to the accumulation effects, the peak gain error after the first section becomes three times larger. Since the peak gain frequency of the first section is located in the stopband of the other sections, however, the accumulation effect becomes less and less significant after four sections. This leads to a saturated error of 57–69% in the back sections. To minimize the errors, the coefficients c_k in the ideal transfer functions can be set slightly smaller than the coefficients c_k used to calculate the corresponding capacitor ratios by a factor 0.96. The results are listed in Table I(b) where the peak gain errors are reduced to be less than 10%. As for the errors of the peak frequencies, they are small in both cases.

V. CONCLUSION

In this paper, new design methodology and multiplexing SC circuits have been proposed to realize a real cochlea. At the cost of the increase in the number of clock phases, the decay slope in the transition band can be sharper with the addition of only a few components. Therefore, the components and chip area of the realized silicon cochlea is small. According to the measured results of the fabricated chips, it has the advantages of large dynamic range and low sensitivity to the process variations. This makes the circuit more realizable in VLSI (very large scale integration). As compared both simulation and experimental results with the data measured from a real cochlea, it has been verified that the designed silicon cochlea can realize the essential features of a real cochlea and reproduce, at least quantitatively, the frequency response of the auditory periphery.

In future work, the circuits of the inner hair cells and the artificial neural network which is connected to the electronic cochlea and performs speech recognition will be investigated and implemented.

ACKNOWLEDGMENT

The authors would like to acknowledge the reviewers for the valuable suggestions and comments which led to substantial improvements in the paper. The assistance of chip manufacture by Chip Implementation Center (CIC), Taiwan, ROC, is also appreciated.

REFERENCES

[1] R. F. Lyon and C. Mead, "An analog electronic cochlea," *IEEE Trans. Acoust., Speech, Signal Processing,* vol. ASSP-36, pp. 1119–1134, July 1988.
[2] L. Watts, D. A. Kerns, R. F. Lyon, and C. A. Mead, "Improved implementation of the silicon cochlea," *IEEE J. Solid-State Circuits,* vol. 27, pp. 692–700, May 1992.
[3] L. Watts, R. Lyon, and C. Mead, "A bidirectional analog VLSI cochlear model," in *Proc. 1991 Santa Cruz Conf. Advanced Res. VLSI,* 1991, pp. 153–163.
[4] W. Liu, A. G. Andreou, and M. H. Goldstein, Jr., "Voiced-speech representation by an analog silicon model of the auditory periphery," *IEEE Trans. Neural Networks,* vol. 3, pp. 477–487, May 1992.
[5] J. J. Zwislocki, "Theory of the acoustical action of the cochlea," *J. Acoust. Soc. Amer.,* vol. 22, pp. 778–784, 1950.
[6] C. Abel, J. Park, M. Ismail, B. Lohiser, S. Justice, S. Bibyk, and T. Fiez, "A switched-current silicon cochlea," in *Proc. IEEE Int. Conf. Neural Network,* Orlando, FL, 1994, pp. 1842–1847.
[7] C.-Y. Wu and J.-C. Bor, "An analog electronic cochlea using multi-clock switched-capacitor circuits," in *Proc. 1991 Int. Symp. IC Design, Manufacture, Applicat.,* Singapore, Sep. 1991, pp. 319–323.
[8] C.-Y. Wu, J.-C. Bor, and B.-S. Jeng, "Realizations of high-order switched-capacitor filters using multiplexing techniques," accepted by *IEEE Trans. Circuits Syst. II: Analog Digital Signal Processing,* vol. 41, no. 12, pp. 778–785, Dec. 1994.
[9] M. Holmes and J. D. Cole, "Pseudoresonance in the cochlea," in *Mechanics of Hearing,* E. de Boer and M. A. Viergever, Eds. The Hague, The Netherlands: Martinus Nijhoff, 1983.
[10] G. Zweig, R. Lipes, and J. R. Pierce, "The cochlear compromise," *J. Acoust. Soc. Amer.,* vol. 59, pp. 975–982, Apr. 1976.
[11] W. S. Rhode, "Observations of the vibration of the basilar membrane in squirrel monkeys using the Mössbauer technique," *J. Acoust. Soc. Amer.,* vol. 49, pp. 1218–1231, 1971.
[12] D. O'Shaughnessy, *Speech Communication: Human and Machine.* Reading, MA: Addison-Wesley, 1987.
[13] P. Allen and E. Sanchez-Sinencio, *Switched-Capacitor Circuits.* New York: Van Nostrand Reinhold, 1984.
[14] R. Gregorian and G. C. Temes, *Analog MOS Integrated Circuits for Signal Processing,* ch. 5. New York: Wiley, 1986.
[15] C.-Y. Wu, T.-C. Yu, and S.-S. Chang, "New monolithic switched-capacitor differentiators with good noise reject," *IEEE J. Solid-State Circuits,* vol. 24, pp. 177–180, Feb. 1989.
[16] ——, "Realization of IIR/FIR and N-path filters using a novel switched-capacitor technique," *IEEE Trans. Circuits Syst.,* vol. 37, pp. 91–106, Jan. 1990.
[17] B. J. Hosticka, R. W. Brodersen, and P. R. Grey, "MOS sampled-data recursive filters using switched capacitor integrators," *IEEE J. Solid-State Circuits,* vol. SC-12, pp. 600–608, Dec. 1977.
[18] J. Lazzaro, "A silicon model of an auditory neural representation of spectral shape," *IEEE J. Solid-State Circuits,* vol. 26, pp. 772–777, May 1991.
[19] J. B. Allen, "Cochlear modeling," *IEEE ASSP Mag.,* pp. 3–29, Jan. 1985.
[20] C. A. Mead, *Analog VLSI and Neural Systems.* Reading, MA: Addison-Wesley, 1989.
[21] R. F. Lyon, "A computational model of filtering, detection, and compression in the cochlea," in *Proc. IEEE Int. Conf. Acoust., Speech, Signal Processing,* Paris, France, 1982, pp. 1282–1285.
[22] R. F. Lyon and L. Dyer, "Experiments with a computational model of the cochlea," in *Proc. IEEE Int. Conf. Acoust., Speech, Signal Processing,* Tokyo, Japan, 1986, pp. 1975–1978.
[23] L. Deng and C. D. Geisler, "A composite auditory model for processing speech sounds," *J. Acoust. Soc. Amer.,* vol. 82, pp. 2001–2012, Dec. 1987.
[24] E. de Boer and E. van Bienema, "Solving cochlear mechanics problems with higher-order differential equations," *J. Acoust. Soc. Amer.,* vol. 72, pp. 1427–1434, Nov. 1982.
[25] J. B. Allen and M. M. Sondhi, "Cochlear macromechanics: Time domain solutions," *J. Acoust. Soc. Amer.,* vol. 66, pp. 123–132, July 1979.
[26] M. R. Schroeder, "An integrable model for the basilar membrane," *J. Acoust. Soc. Amer.,* vol. 53, pp. 429–434, 1973.

Jenn-Chyou Bor was born in Hualian, Taiwan, Republic of China, in 1966. He received the B.S. degree from the Department of Electronics Engineering, National Chiao-Tung University, Hsinchu, Taiwan, in 1988. He is currently working toward the Ph.D. degree at the same institute. His main research interests include switched-capacitor filters and neural network integrated circuits and systems.

Chung-Yu Wu (S'76–M'77) was born in Chiayi, Taiwan, Republic of China, in 1950. He received the M.S. and Ph.D. degrees from the Department of Electronics Engineering, National Chiao-Tung University, Taiwan, in 1976 and 1980, respectively.

From 1980–1984, he was an Associate Professor in the National Chiao-Tung University. During 1984–1986, he was a Visiting Associate Professor in the Department of Electrical Engineering, Portland State University, OR. Since 1987, he has been a Professor in the National Chiao-Tung University. He has published more than 50 journal papers and 60 conference papers on several topics, including digital integrated circuits, analog integrated circuits, computer-aided design, neural networks, ESD protection circuits, special semiconductor devices, and process technologies. He also has eight patents including four U.S. patents. His current research interests focus on low-voltage low-power mixed-mode integrated circuit design, hardware implementation of visual and auditory neural systems, and RF integrated circuit design.

Dr. Wu is a member of Eta Kappa Nu and Phi Tau Phi.